

## $\pi N$ - $\pi N$ in J-PARC

### **Proposal on measurements of the spin rotation parameters $A$ and $R$ at the J-PARC in the resonance region of the $\pi N$ -elastic scattering**

(The key experiment in the baryon spectroscopy)

Petersburg Nuclear Physics Institute (Gatchina, Leningrad district)

Institute for Theoretical and Experimental Physics (Moscow)

#### Names of experimentalists:

V.V.Sumachev, S.P.Kruglov, I.V.Lopatin, E.A.Filimonov, N.G.Kozlenko, V.S.Kozlov, D.V.Novinsky,  
A.I.Kovalev, V.Yu.Trautman (PNPI)

I.G.Alekseev, D.N.Svirida, V.P.Kanavets, B.V.Morozov, V.V.Ryltsov, V.M.Nesterov (ITEP)

## $\pi$ N- $\pi$ N in J-PARC

### Abstract

Pion-nucleon interaction leading to the formation of nonstrange baryon resonances is one of fundamental interactions in the elementary particle physics. Nowadays there exists the evident disagreement between the number and characteristics of baryon resonances extracted from experimental data by different partial wave analysis (PWA) collaborations and those predicted by different theoretical models. The difference between PWA results is due amongst other things to the twofold ambiguities, which are inherent to the PWA procedure.

The spin rotation parameters A and R measurements in the pion-nucleon elastic scattering is practically the unique reliable method to exclude the twofold ambiguities from the  $\pi$ N-amplitudes. In 2006 year the new PWA VPI-GWU (SP06) was published. Predictions of this analysis for the spin rotation parameters A and R are deduced by creation of given proposals.

## Introduction.

### 1. Introduction

The baryon resonances were discovered in 1950 year [Y.Fujimoto, H.Miyazawa; Progr. Theor. Phys. 5 (1950) 1052] in the reaction of the photoproduction. T.Nakano, K.Nishigima, M.Gell-Mann in 1953 year introduced the concepts of baryon number  $N_b$  and strangeness  $S$ .

But before now (2006 year) the world scientific community have not a complete picture of the  $\pi N$ -interactions. A uniquely determined  $\pi N$ -amplitude is absent in the resonance region of the  $\pi N$ -interactions. We don't know correctly - how many  $N^*$ ,  $\Delta$ ,  $\Lambda$ ,  $\Sigma$ ,  $\Xi$ ,  $\Omega$  baryons there exist - neither experimentally, nor theoretically. There is no way in which it can be possible to resolve this problem except by a careful experimental study of the all  $\pi N$ -interaction channels in total resonance region. If the high intensity pion beam with corresponding momentum will be realized at J-PARC, it will give the unique possibility to resolve this problem by means of every  $\pi N$  interaction channel experimental investigation.

Historically, the best information came from  $\pi N$  experiments, a situation that still holds now [1]. Pion-nucleon interaction leading to the formation of nonstrange baryon resonances is one of fundamental interactions in the elementary particle physics. The interest in the study of baryon resonances has led to the important discovery of SU(3) symmetry. Just a multi-resonance structure of  $\pi N$ -system has given a power impulse to developing quark-gluon models of baryons. Although many excited states of baryons were found, the quality and scope of the data limited the analyses [2].

## Physics goals.

### 2. Physics Goals

This experiment was aimed at next goals:

- (I) To obtain new experimental data for unambiguous reconstruction of  $\pi p$ -elastic amplitudes in the range of pion beam momentum and angles where the largest disagreement between predictions of the existing PWA's is observed;
- (II) To prove the choice of the transverse amplitude zero trajectory (solution branch);

The specific feature of measurements of the spin rotation parameters is that it is not necessary to make measurements in the full energy and angle ranges. It is enough to measure these parameters in some limited intervals of kinematical variables – that can be determined beforehand on the base of existing PWAs – in order to eliminate the problem of PWA ambiguities.

In Tables 3 and 4 we present these limited intervals of kinematical variables for the second resonance region of  $\pi N$ -elastic scattering, which cover masses of baryon resonances from 1400 to 2000 MeV. The intervals were determined by analyzing zero trajectories of  $\pi N$  transverse amplitudes obtained for four existing global PWAs: KA84 ( $T_\pi = 0.02\text{--}10$  GeV) [4], CMB ( $T_\pi = 0.3\text{--}2.2$  GeV) [3], VPI-GWU solutions FA02 ( $T_\pi = 0\text{--}2.1$  GeV) and SP06 ( $T_\pi = 0\text{--}2.5$  GeV)[5]. In the column 2 and 3 those intervals of laboratory pion momentum and c.m.s. scattering angle are indicated, in which the existence of discrete ambiguities is mostly probable and, hence, measurements of the spin rotation parameters in  $\pi p$  elastic scattering are needed first of all. Expected counting rates can be estimated using values of c.m.s. differential cross sections given in the column 4. A statistical precision at a level of  $\Delta A$  ( $\Delta R$ )  $\approx 0.1$  is enough to distinguish different PWA solutions. The VPI-GWU experimental data volume is:

SP06: P+ = 27190/13344; P- = 22702/11967; CX = 6084/2933;

FA02: P+ = 21735/10468; P- = 18932/9650; CX = 4136/1690;

SM95: P+ = 22616/10197; P- = 18883/9421; CX = 4402/1625;

## $\pi N$ - $\pi N$ in J-PARC

Table 1: Elastic  $\pi^+p$ -scattering  
(Regions with presumed existence of discrete ambiguities)

Number	Momentum region ( MeV/c)	Angle region c.m.s.(deg.)	Diff. cross section (mb/sr)
1	700 – 900	90 - 110	0.03 - 0.18
2	800 – 1000	155 – 175	0.08 – 0.60
3	800 – 1200	80 – 100	0.13 – 0.27
4	1600 – 1900	50 – 70	0.08 – 0.30
5	1800 – 2100	130 - 150	0.03 – 0.13

Table 2: Elastic  $\pi^-p$ -scattering  
(Regions with presumed existence of discrete ambiguities)

Number	Momentum region ( MeV/c)	Angle region c.m.s.(deg.)	Diff. cross section (mb/sr)
1	600 – 800	60 - 80	0.06 - 0.20
2	600 – 800	100 – 120	1.0 – 1.4
3	1200 – 1400	150 – 170	0.30 – 0.53
4	1200 – 1500	60 – 80	0.05 – 0.23
5	1200 - 1500	90 - 110	0.25 – 0.40
6	1800 – 2100	140 - 150	0.002 – 0.010
7	2000 - 2100	130 - 150	0.001 – 0.003

# $\pi N$ - $\pi N$ in J-PARC

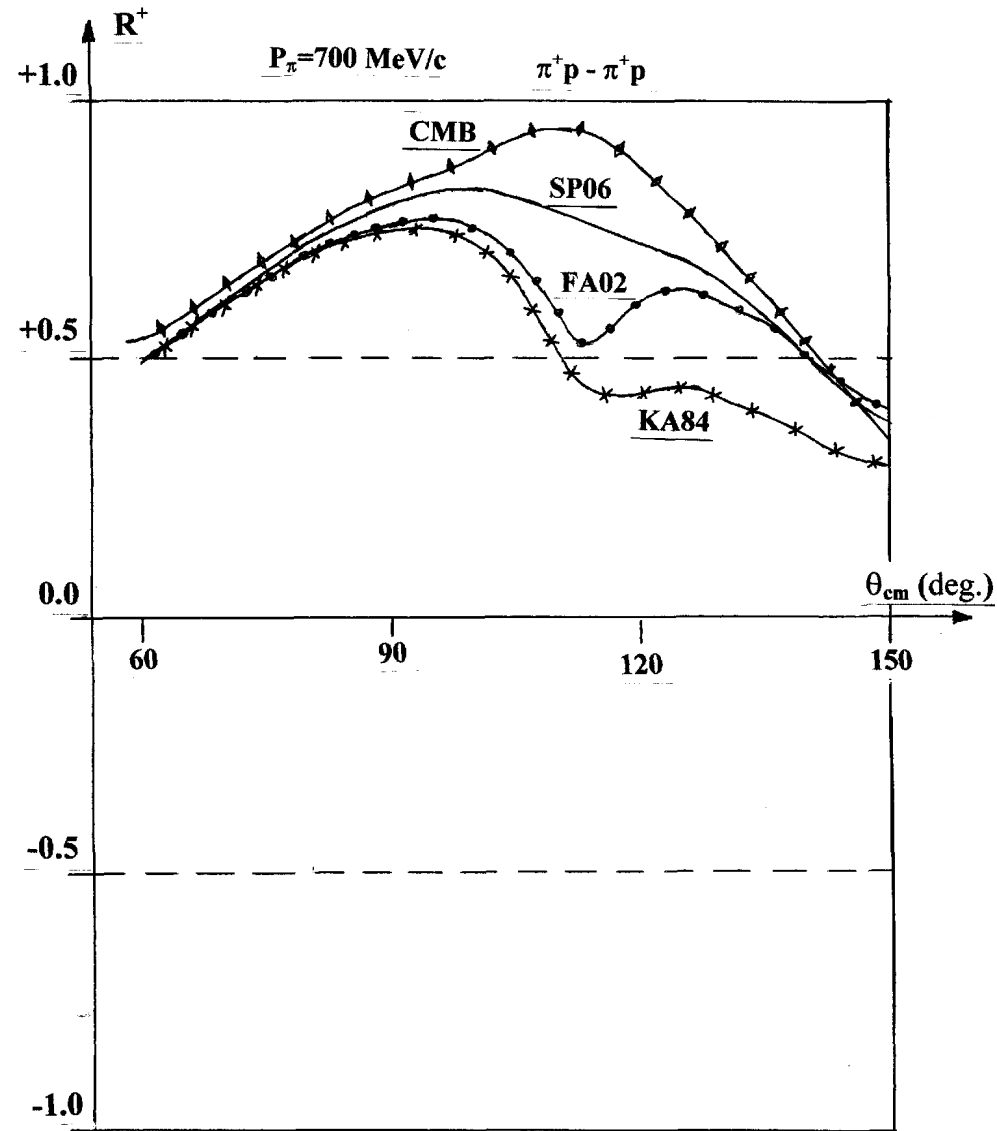


Figure 1. Comparison of PWA's predictions for  $\pi^+ p$  elastic scattering at  $P_\pi = 700$  MeV/c.

# $\pi N - \pi N$ in J-PARC

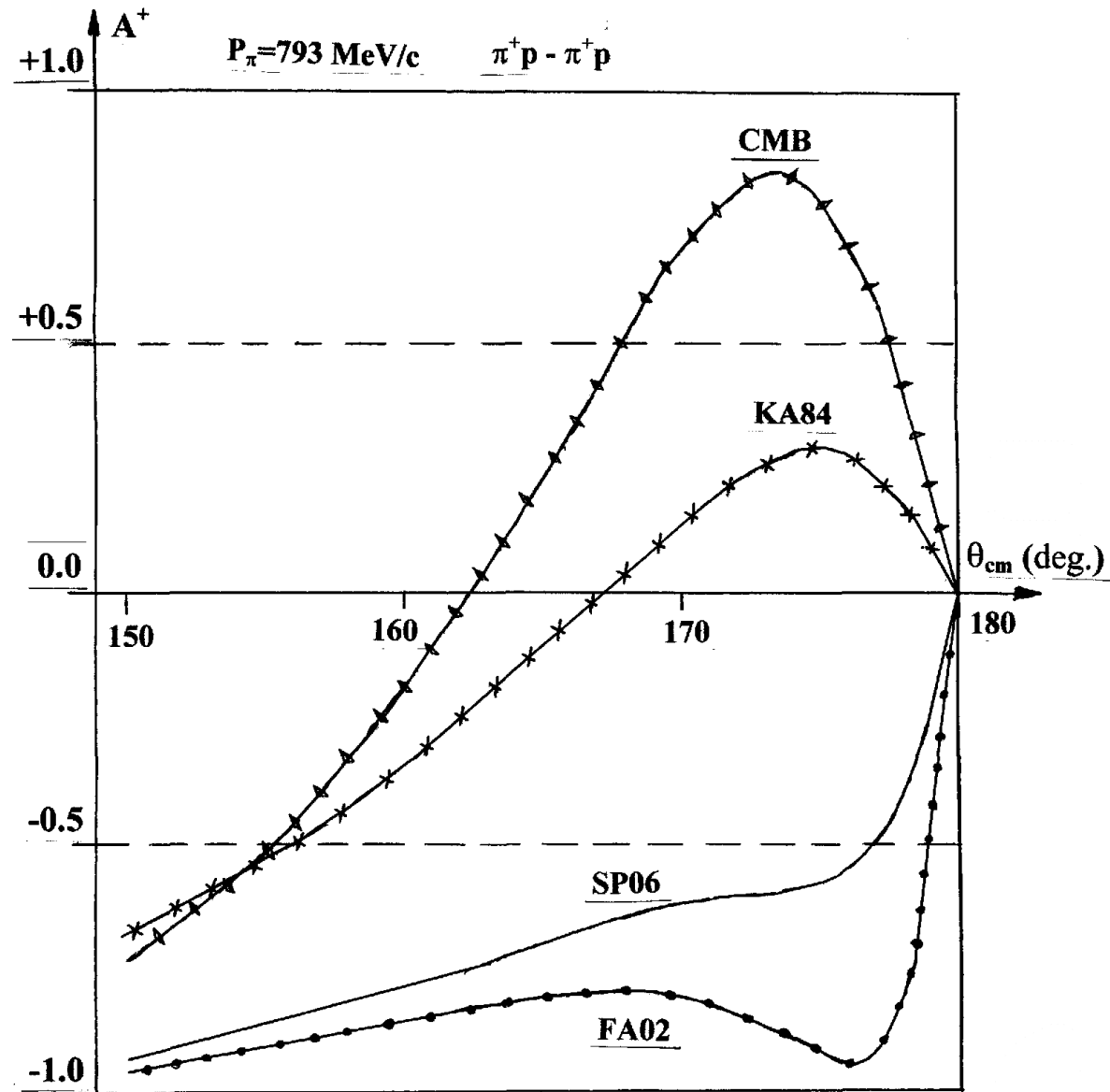


Figure 2. Comparison of PWA's predictions for  $\pi^+ p$  elastic scattering at  $P_\pi = 793 \text{ MeV}/c$ .

# $\pi N - \pi N$ in J-PARC

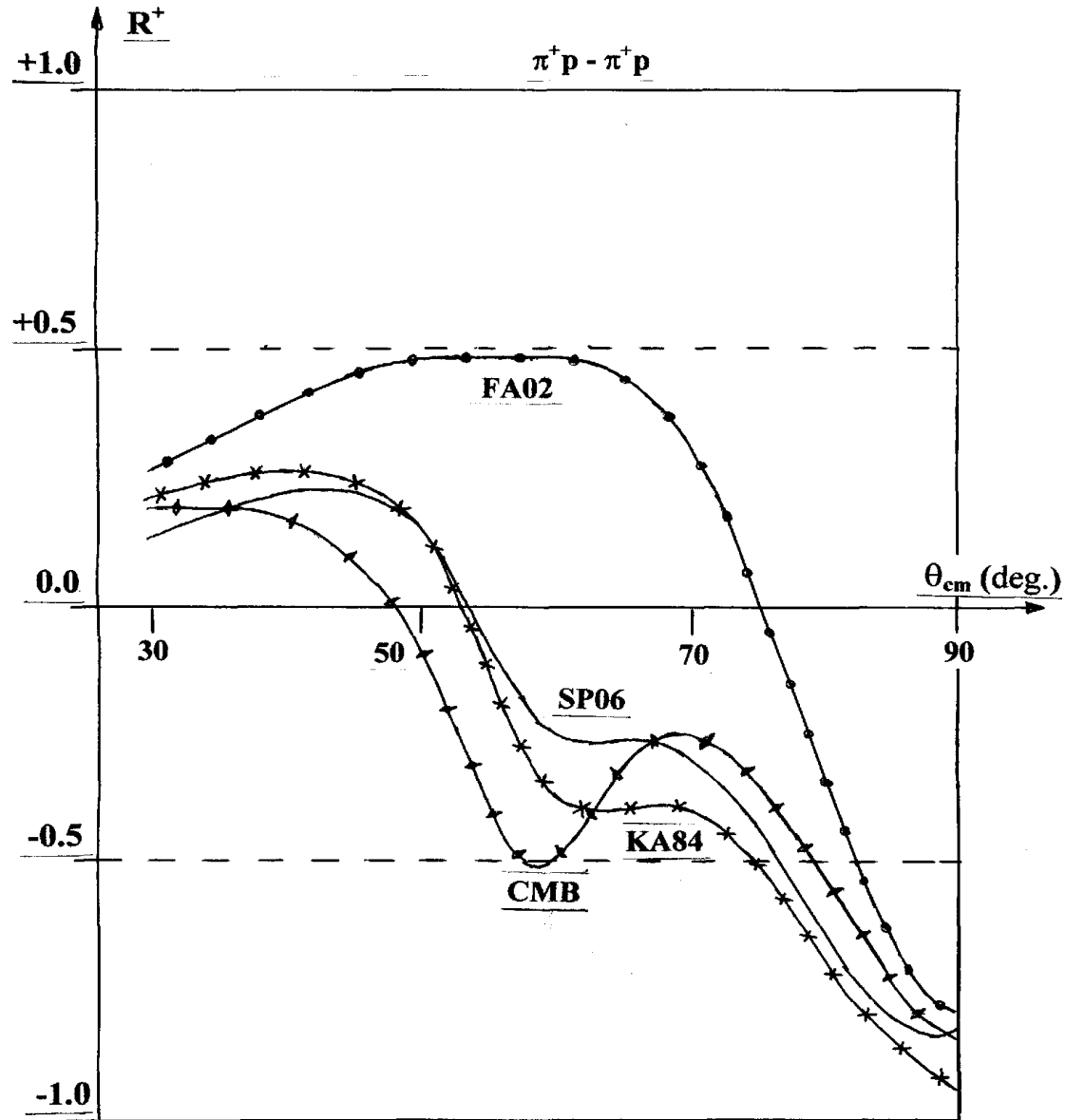


Figure 3. Comparison of PWA's predictions for  $\pi^+ p$  elastic scattering at  $P_\pi = 1700$  MeV/c.



# $\pi N - \pi N$ in J-PARC

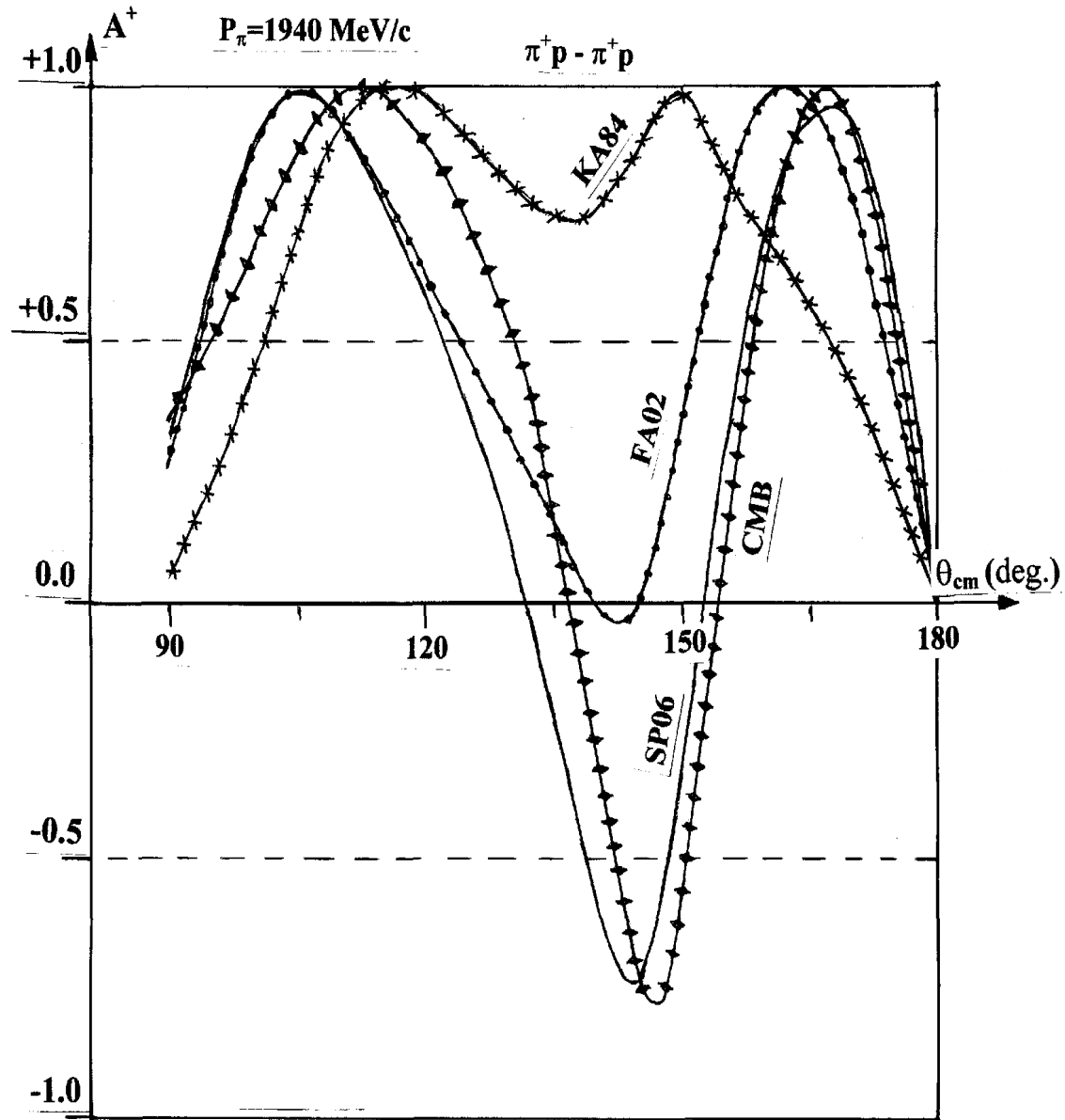


Figure 4. Comparison of PWA's predictions for  $\pi^+ p$  elastic scattering at  $P_\pi = 1940$  MeV/c.

$\pi N$ - $\pi N$  in J-PARC

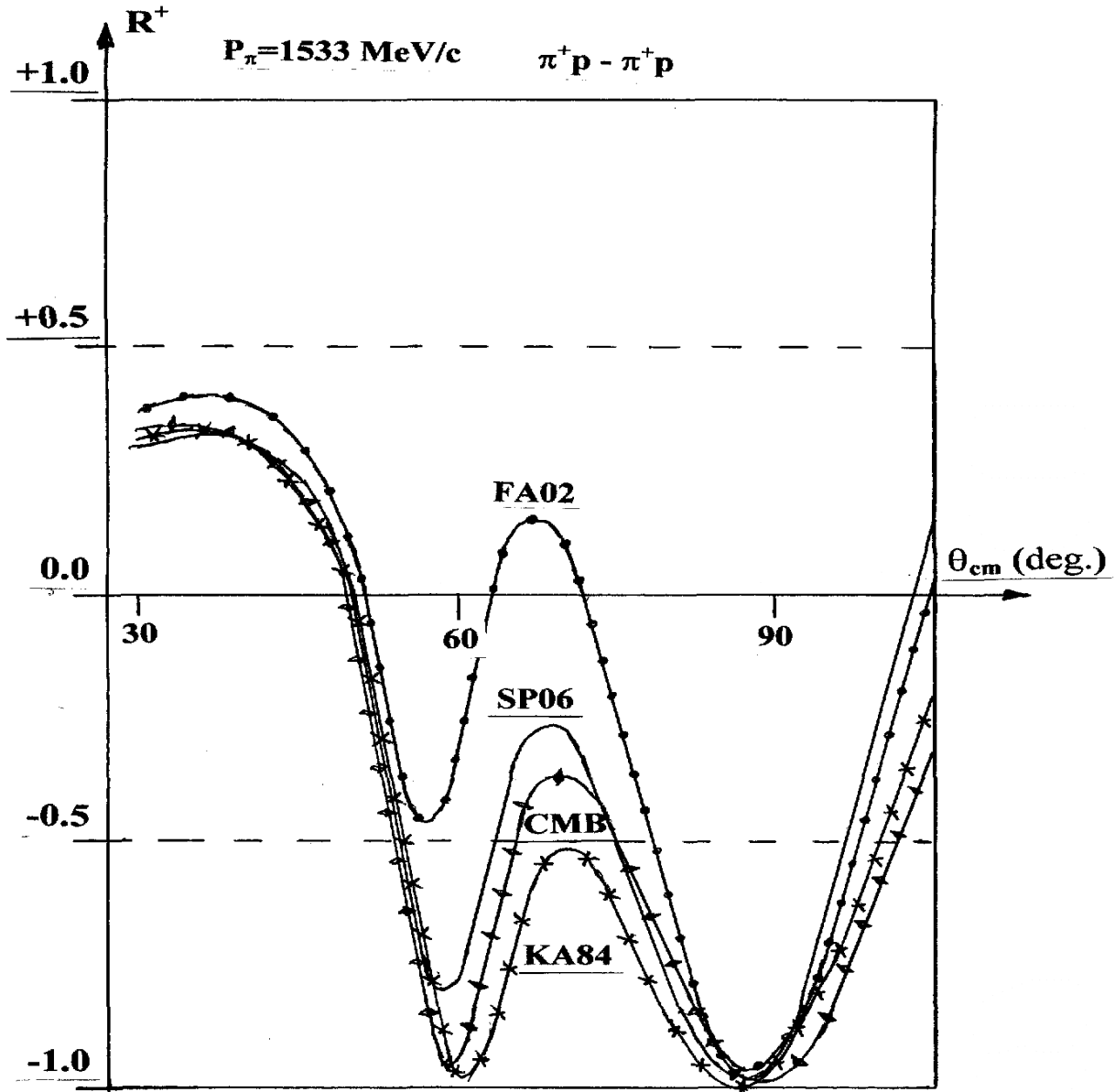


Figure 5. Comparison of PWA's predictions for  $\pi^+ p$  elastic scattering at  $P_\pi = 1533 \text{ MeV/c}$ .

# $\pi N - \pi N$ in J-PARC

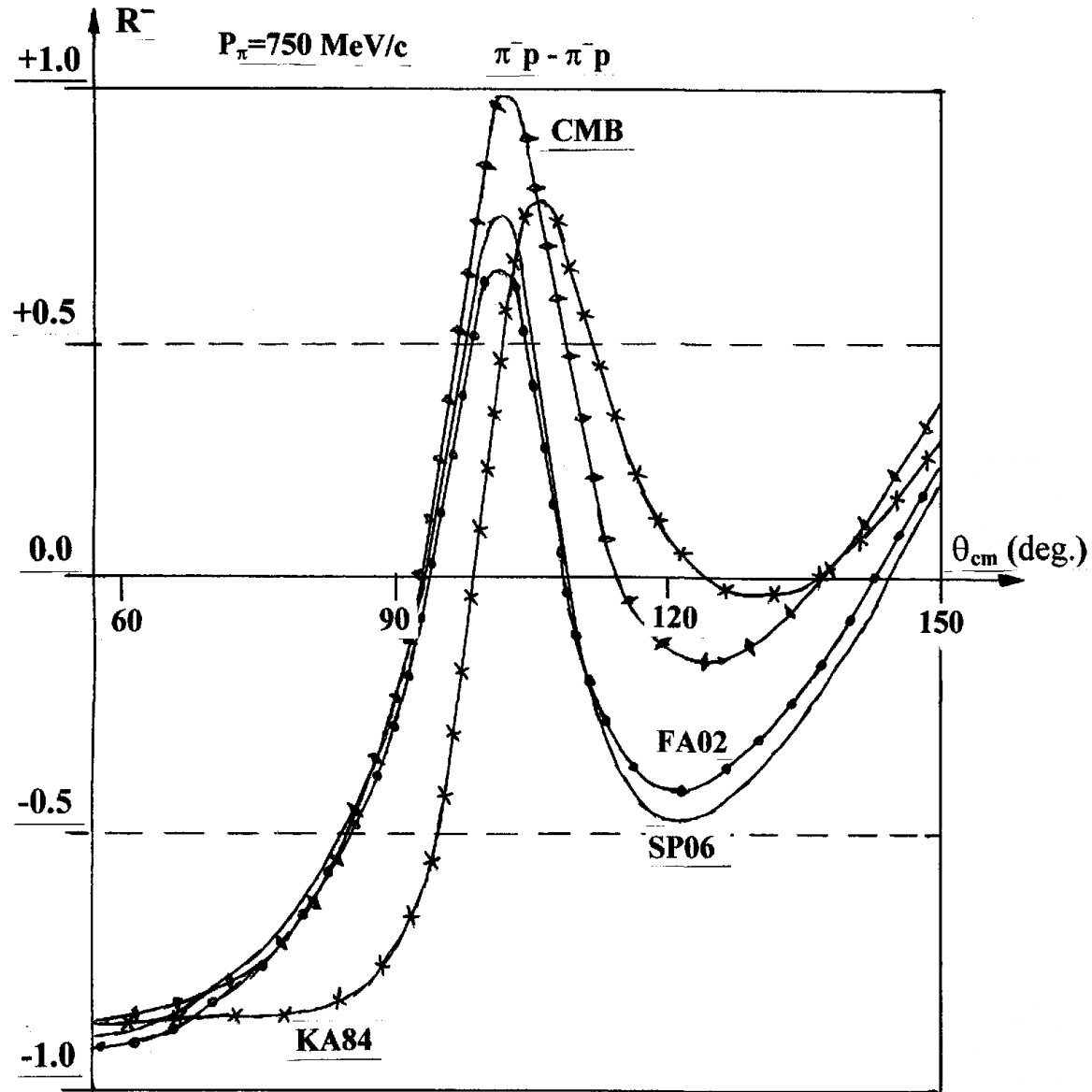


Figure 6. Comparison of PWA's predictions for  $\pi^- p$  elastic scattering at  $P_\pi = 750$  MeV/c.

# $\pi N - \pi N$ in J-PARC

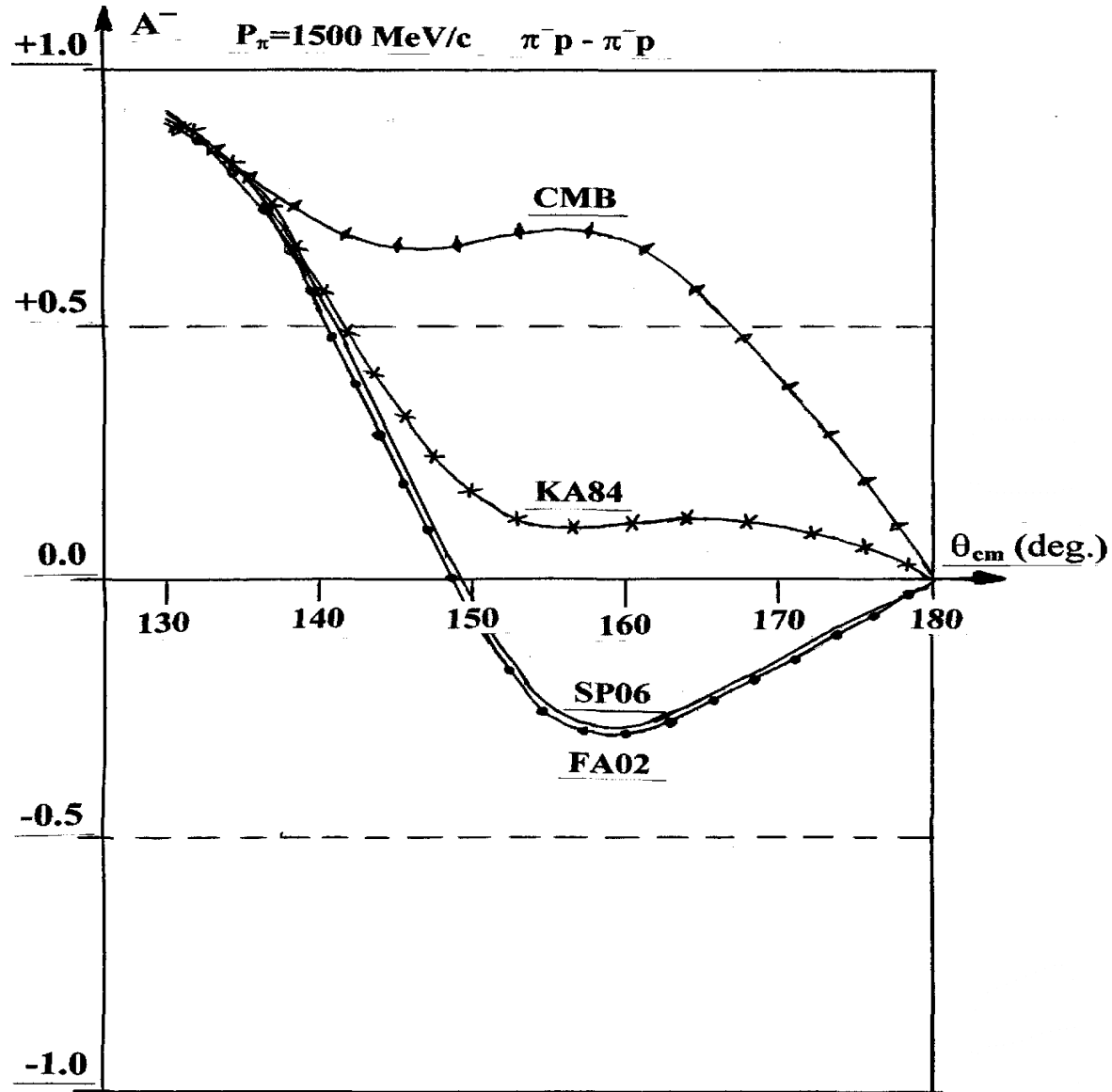


Figure 7. Comparison of PWA's predictions for  $\pi^- p$  elastic scattering at  $P_\pi = 1500 \text{ MeV}/c$ .

# $\pi N - \pi N$ in J-PARC

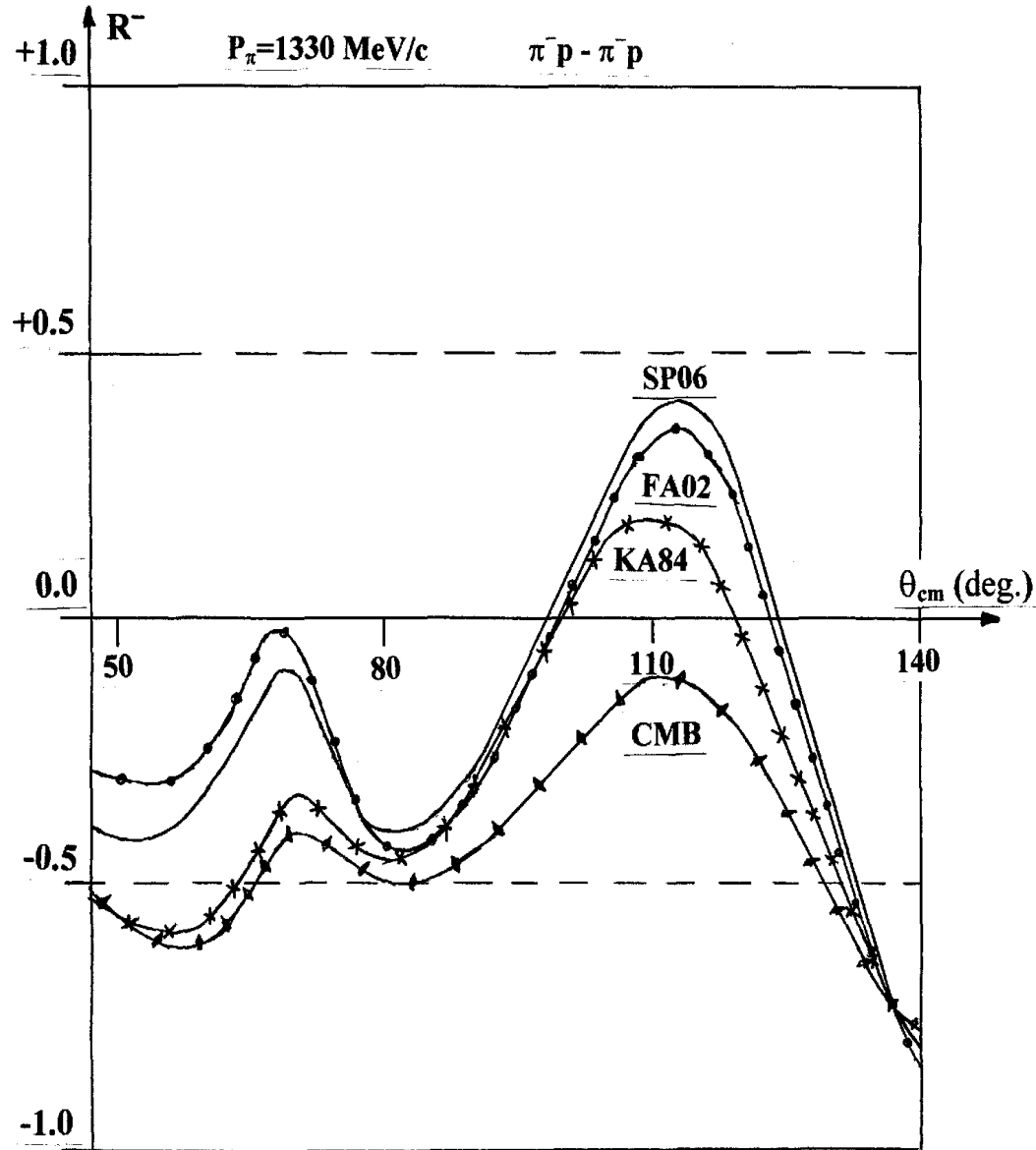


Figure 8. Comparison of PWA's predictions for  $\pi^- p$  elastic scattering at  $P_\pi = 1330 \text{ MeV}/c$ .

# $\pi N$ - $\pi N$ in J-PARC

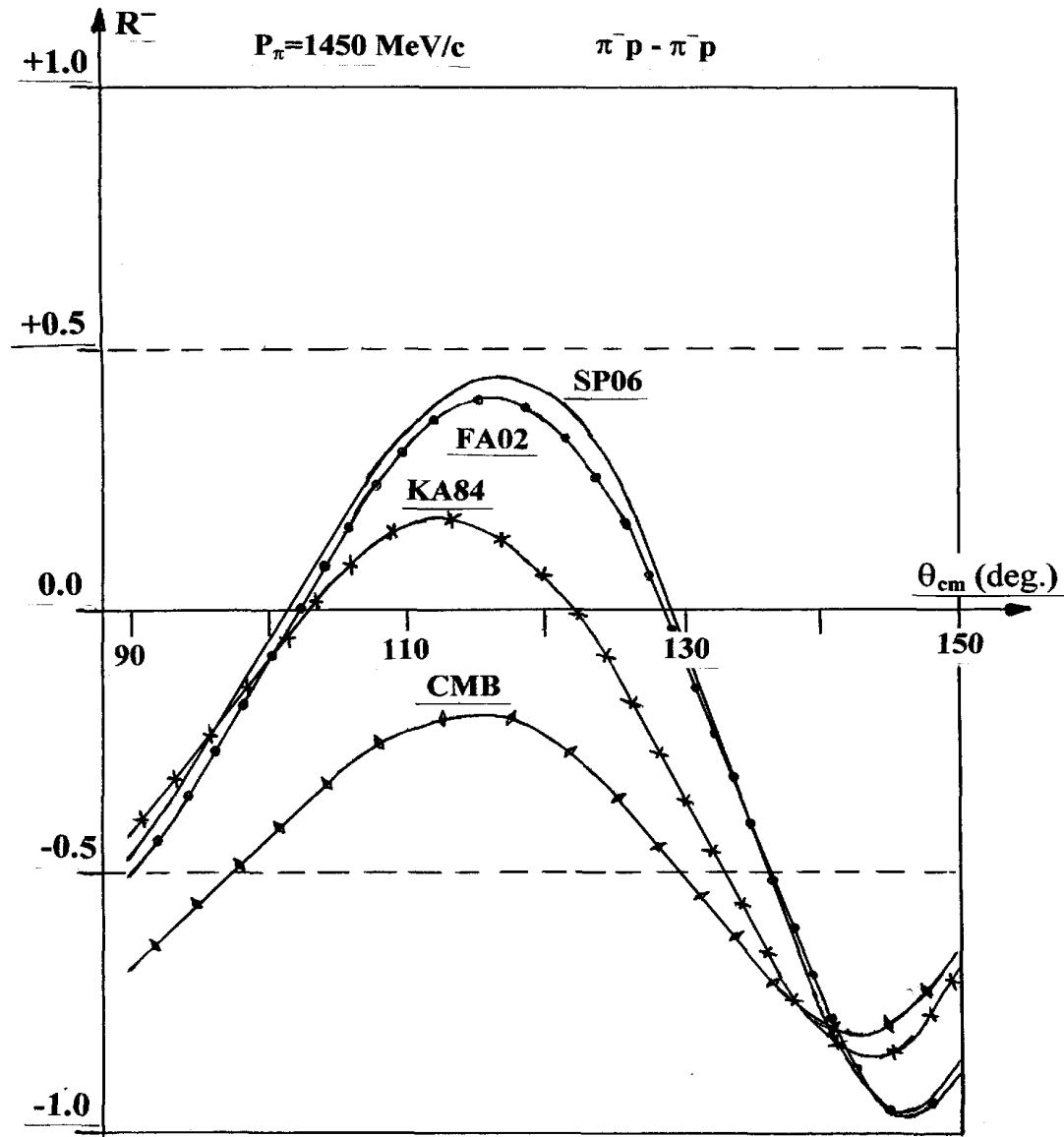


Figure 9. Comparison of PWA's predictions for  $\pi^-p$  elastic scattering at  $P_\pi=1450$  MeV/c.

# $\pi N$ - $\pi N$ in J-PARC

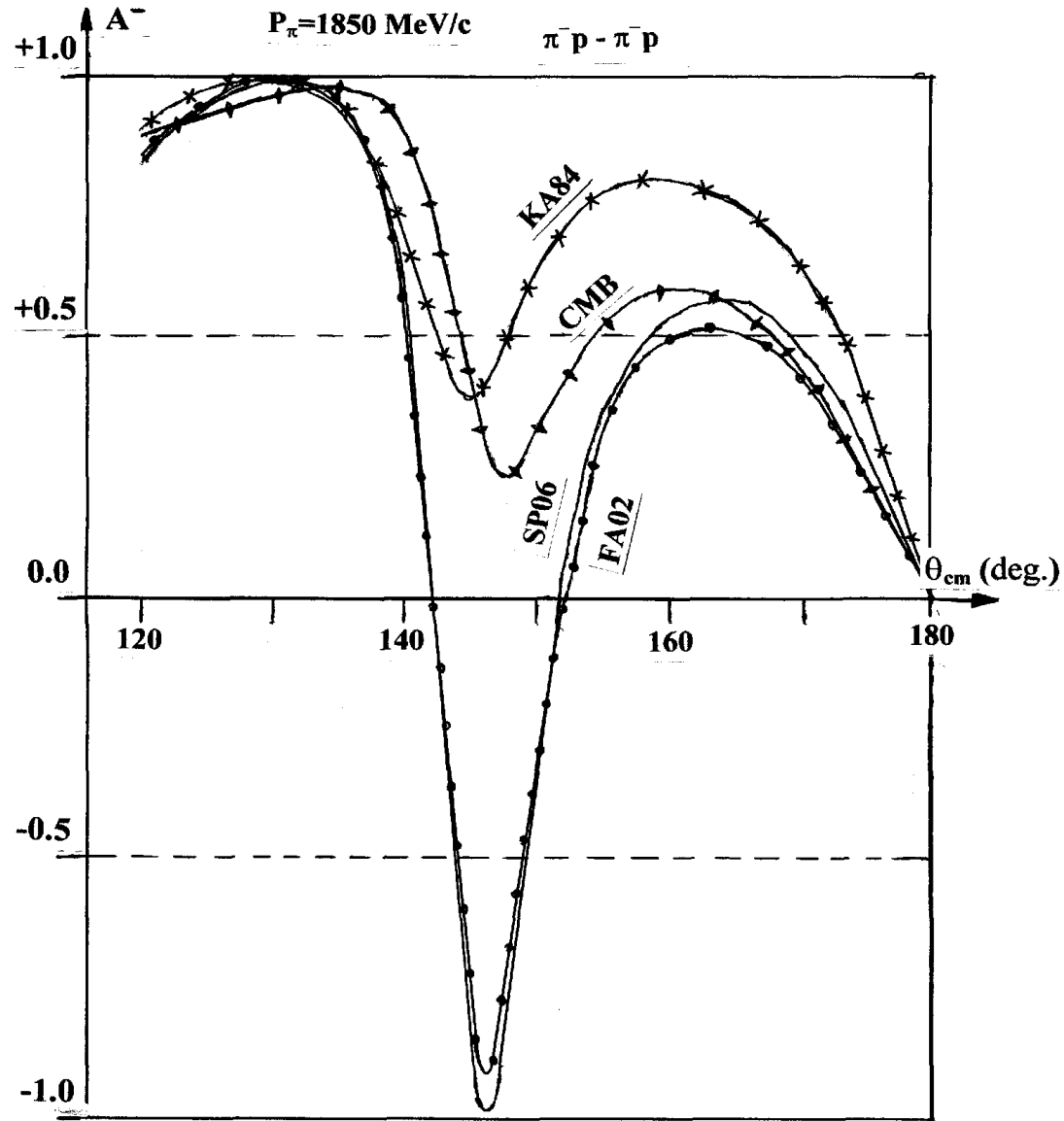


Figure 10. Comparison of PWA's predictions for  $\pi^- p$  elastic scattering at  $P_\pi = 1850$  MeV/c.

$\pi N$ - $\pi N$  in J-PARC

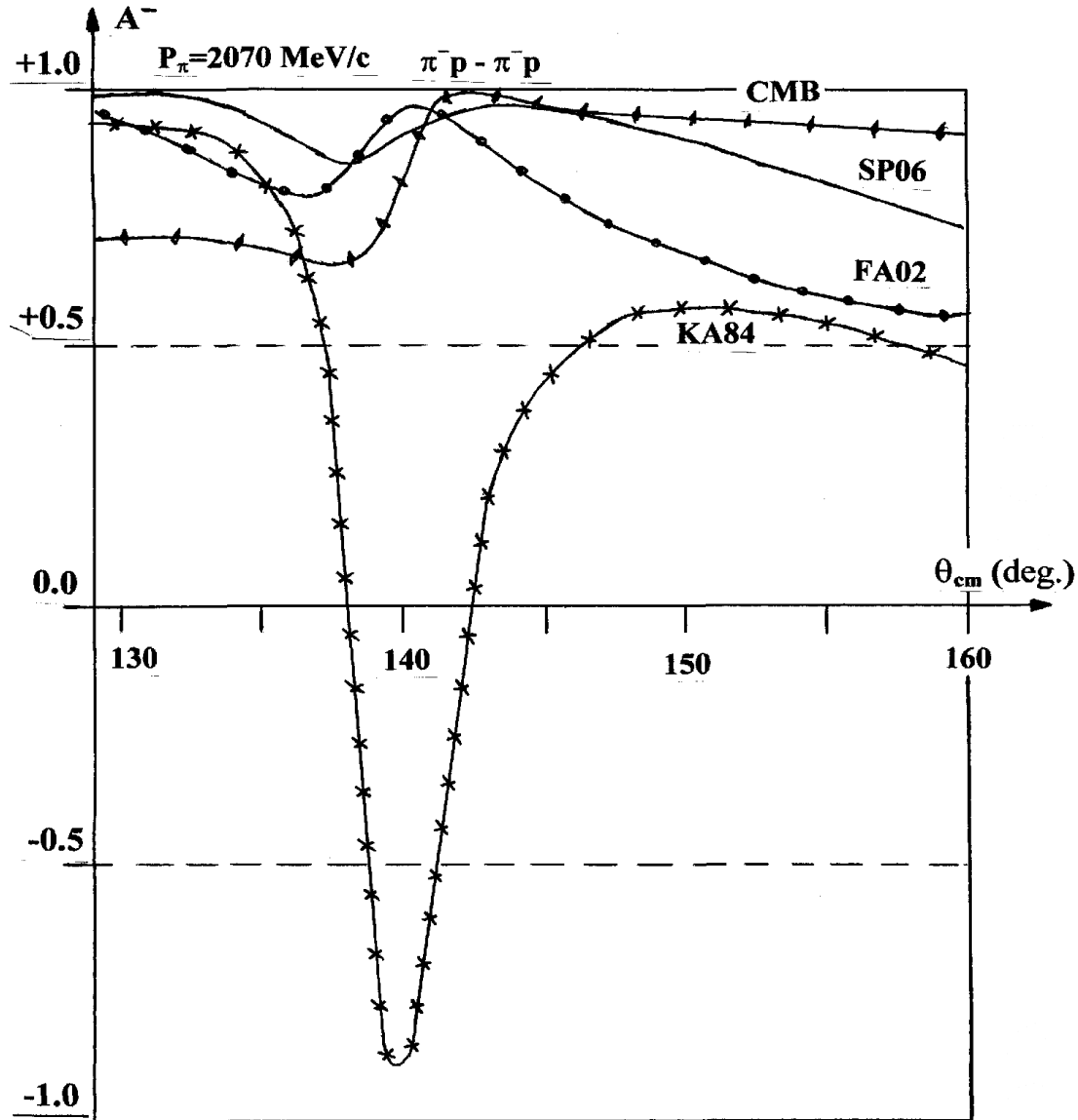


Figure 11. Comparison of PWA's predictions for  $\pi^- p$  elastic scattering at  $P_\pi = 2070$  MeV/c.



## Experimental setup.

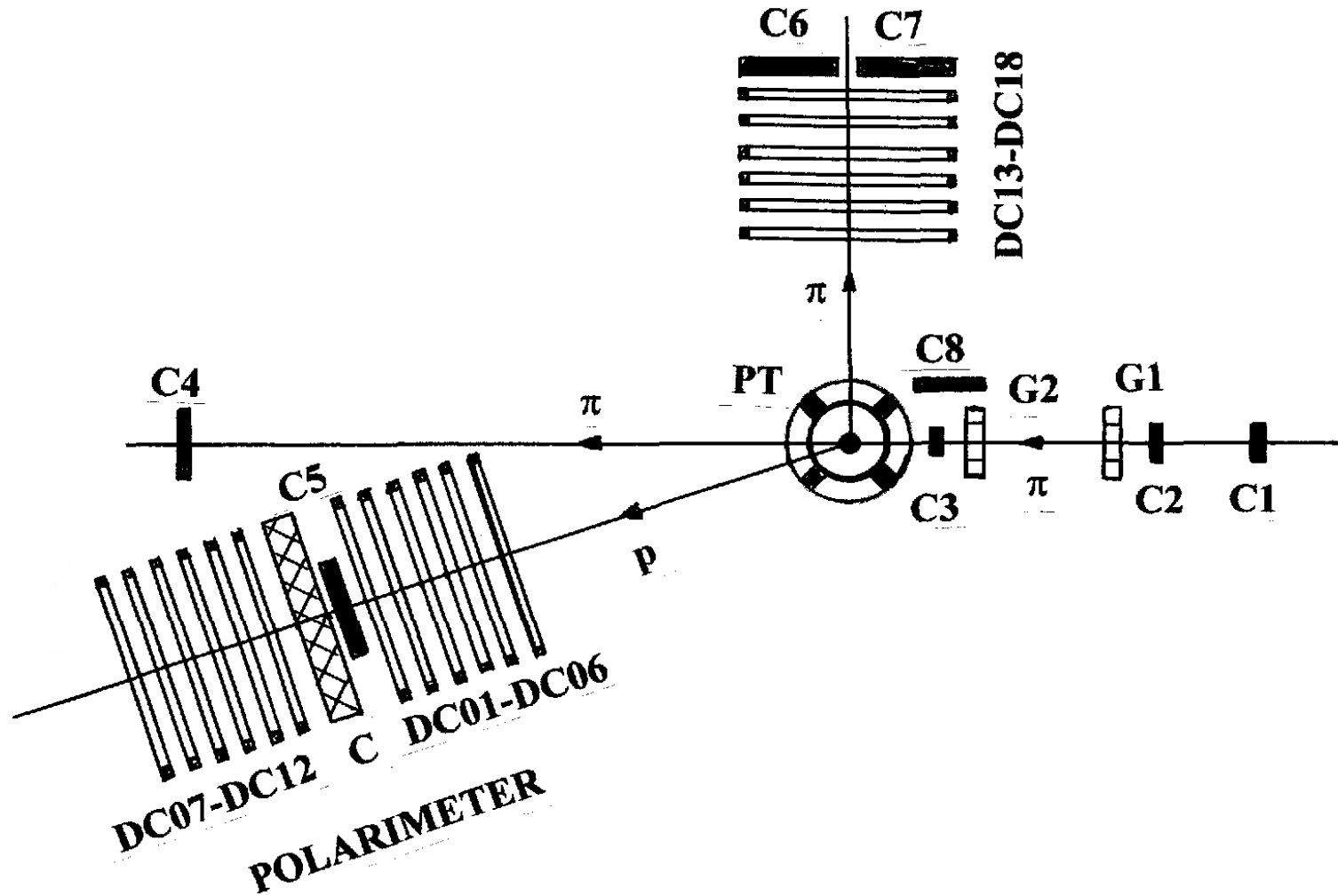
### 3. Experimental setup “SPIN-PMJ”

The spin rotation parameters  $A$  and  $R$  in  $\pi N$  elastic scattering are determined by the measurement of the polarization of recoiled protons produced by pions on a proton target polarized in the scattering plane. Polarization of the recoiled protons is measured through the asymmetry of their secondary scattering on the analyzing substance (carbon).

The apparatus is shown in Fig.12. Its basic elements are:

- (i) Polarized proton target (PT);
- (ii) Proton polarimeter included carbon filter (C), six sets of drift chambers (DC01-DC06) to detect the recoiled proton before and six sets of drift chambers (DC07-DC12) to detect the recoiled proton after pC-scattering;
- (iii) Six sets of drift chambers to detect the scattered pion (DC13-DC18);
- (iv) Two pion beam multichannel hodoscopes G1 and G2;
- (v) A number of scintillation counters (C1-C8) to provide the trigger and to identify the positive pions in the beam by the time of flight.

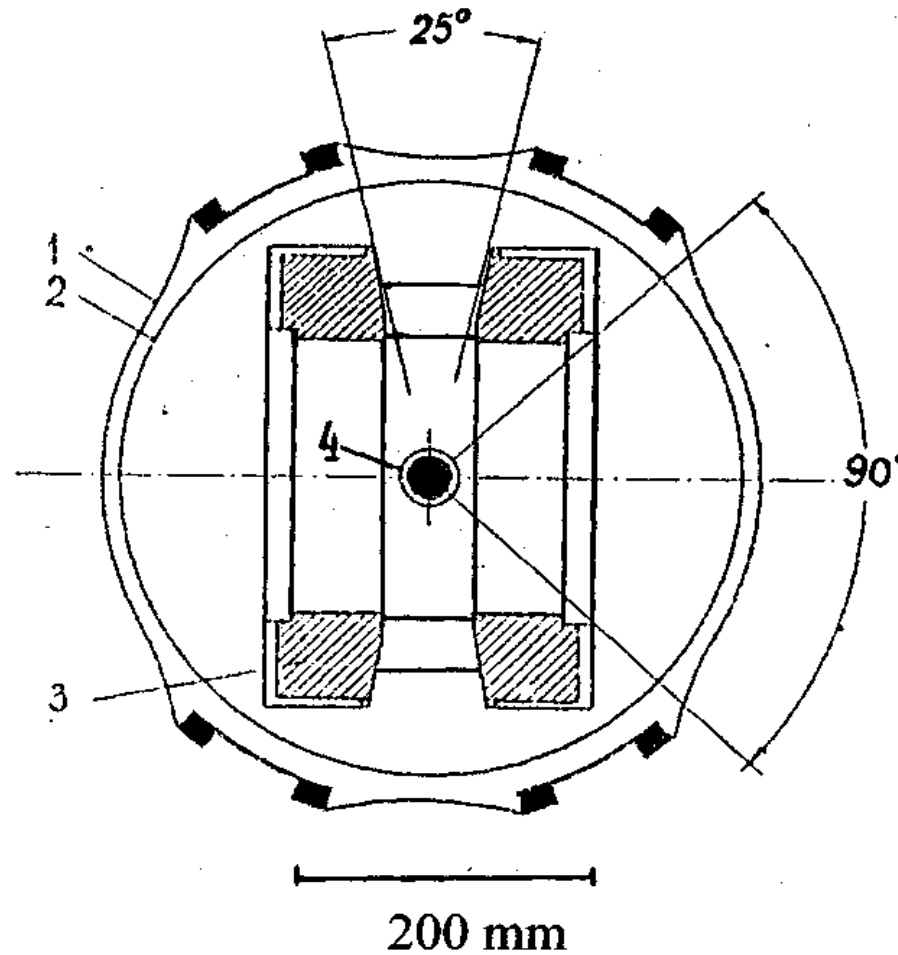
$\pi$ N- $\pi$ N in J-PARC



**The experimental layout SPIN-PMJ (not to scale).**

Figure 12. SPIN-PMJ setup. PT – polarized target; C1-C8 – scintillation counters; G1, G2 – beam hodoscopes; DC01 – DC18 – drift chambers; C – carbon scatterer.

$\pi N$ - $\pi N$  in J-PARC



Polarized target section by horizontal plane.

Figure 13. 1 – window (stainless steel, 0.1 mm); 2 – nitrogen screen (aluminum, 0.1 mm); 3 – magnet; 4 – appendix with a container filled with the target material (aluminum alloy, 0.4 mm)

### 3.1. Polarized Target

The polarized proton target with arbitrary spin orientation in the horizontal plane has been built at PNPI especially for the measurements of the spin rotation parameters in the  $\pi$ p-elastic scattering (Fig.13.). A container filled with the target material (propanediol  $C_3H_8O_2$  doped by  $Cr^V$  complexes) is placed into magnetic field of 2.5 T created by a Helmholtz pair of superconductive coils [11].

The container has a cylindrical form with vertical size and diameter of 30 mm x 30 mm. Cooling of the target down to 0.5 K is provided by an evaporation-type  $^3He$ -cryostat. The polarization is pumped by the dynamic nuclear orientation method up to the absolute value of 70-80 % with an uncertainty of 1.5 %. The method of proton magnetic resonance (PMR) is used for the polarization measurements. These measurements are based on the calculations of area under the PMR curve. The equipment is calibrated on the equilibrium target polarization at temperature of 0.5 K.

### 3.2. Proton polarimeter

Recoil proton polarimeter consists of two sets of one-coordinate drift chambers (six chambers in each set) and carbon block. The accuracy of determinations of the secondary scattering angle is near  $1^\circ$ .

The average analyzing power for selected events is usually between 0.1 – 0.3. For realization of presented proposal it is necessary to have possibility to measure the normal components of recoil proton polarization in the proton energy range from 100 to 1600 MeV and to know the pC-analyzing power in this energy region. The PNPI-ITEP collaboration performed the associated investigations. At the first step the existing till now world experimental data were collected and pC-analyzing power has been investigated as a function of proton scattering angle  $\theta_{pC}$ , proton kinetic energy  $T_p$  and energy losses in the process pC-scattering  $E'$  in this energy range [12]. At the next step the pC analyzing power for polarized protons has been experimentally measured by PNPI-ITEP collaboration for proton beam momentum of 1.36, 1.60, 1.78 and 2.02 GeV/c and for carbon scatterer thickness of 4.9, 19.4 and 36.5 g/cm<sup>2</sup>. These data have been compared with previous results [12] and used to fit analyzing power obtained for various proton energies and scattering angles [13]. For the spin rotation parameters A and R measurements the thickness of carbon blocks will be optimized in accordance with recoil proton energy and range [12].

The carbon (graphite GMZ) is 99.9% pure.

4

**5.Experimental setup “SPIN-PMJ” arrangement at J-PARC pion beam.**

The distance between polarized target and last magnet element of the pion channel should be more than 3 m for the beam pion direction determinations.

The height of the polarized target container over the experimental hall floor should be more than 1.3 m. This is defined by PT constructions.

The full size of the experimental setup is 6 m perpendicularly to the pion beam (3m+3m) and 8 m along the pion beam.

It is necessary that the full height of the experimental hall must be more than 3.5 m in the SPIN-PMJ setup region for the polarized target service.

### 4. Conclusion

The experimental program includes the measurement of the spin rotation parameters A and R at 7-8 MeV, where the existence of discrete ambiguities is mostly probable. These data will be used in performing the new PWA for obtaining the unambiguous behavior of a zero trajectory at “critical points” [6] and to exclude the twofold ambiguities from the  $\pi N$ -amplitudes.

After this procedure, some additional measurements can be necessary for a completion of the elastic channel investigation in the baryon resonance region.

In the following, the main elements of SPIN-PMJ experimental set can be used for the investigation of the polarization parameters in the other channels of the pion-nucleon interactions in the resonance region [1,16].

Today the collaboration has the polarized target and scintillation counters. The drift chambers are being designed. The cost of the first two DC production is near 7200 Euro, every next two DC cost is estimated as 5400 Euro. The price of all 18 DC for SPIN-PMJ is estimated near 50400 Euro. The cost of two hodoscopes production is estimated near 9400 Euro.

## πN-πN in J-PARC

Table 1: Parameters of the N\* - resonances.

PDG (2002)	$L_{1,2J}$	Status	KA84 (1984)	$(^3P_0)$ model (1994)	SM95 (1995)	FA02 (2003)	Skyrme (1985)
N(1440)	$P_{11}$	****	1410(135)	1540	1467(440)	1468(360)	----
N(1520)	$D_{13}$	****	1519(114)	1495	1515(106)	1516(98)	1715
N(1535)	$S_{11}$	****	1526(120)	1460	1535(66)	1547(178)	1478
N(1650)	$S_{11}$	****	1670(180)	1535	1667(90)	1651(130)	----
----	$S_{11}$	----	----	----	1712(174)	----	----
N(1675)	$D_{15}$	****	1679(120)	1630	1673(154)	1676(152)	1744
N(1680)	$F_{15}$	****	1684(128)	1770	1678(126)	1683(134)	1823
N(1700)	$D_{13}$	***	1731(110)	1625	----	----	----
N(1710)	$P_{11}$	***	1723(120)	1770	[1770-i189]	----	1427
N(1720)	$P_{13}$	****	1710(190)	1795	1820(354)	1750(256)	1982
N(1900)	$P_{13}$	**	----	1870	----	----	----
----	$P_{11}$	----	----	1880	----	----	----
----	$P_{13}$	----	----	1910	----	----	----
----	$P_{13}$	----	----	1950	----	----	----
----	$P_{11}$	----	----	1975	----	----	----
----	$F_{15}$	----	----	1980	----	----	----
N(1990)	$F_{17}$	**	2005(350)	1980	----	----	2011
N(2000)	$F_{15}$	**	1882(95)	1995	1814(176)	----	----
----	$P_{13}$	----	----	2030	----	----	----
----	$S_{11}$	----	----	2030	----	----	----
----	$D_{13}$	----	----	2055	----	----	----



## πN-πN in J-PARC

**Table 2. Parameters of the Δ – resonances.**

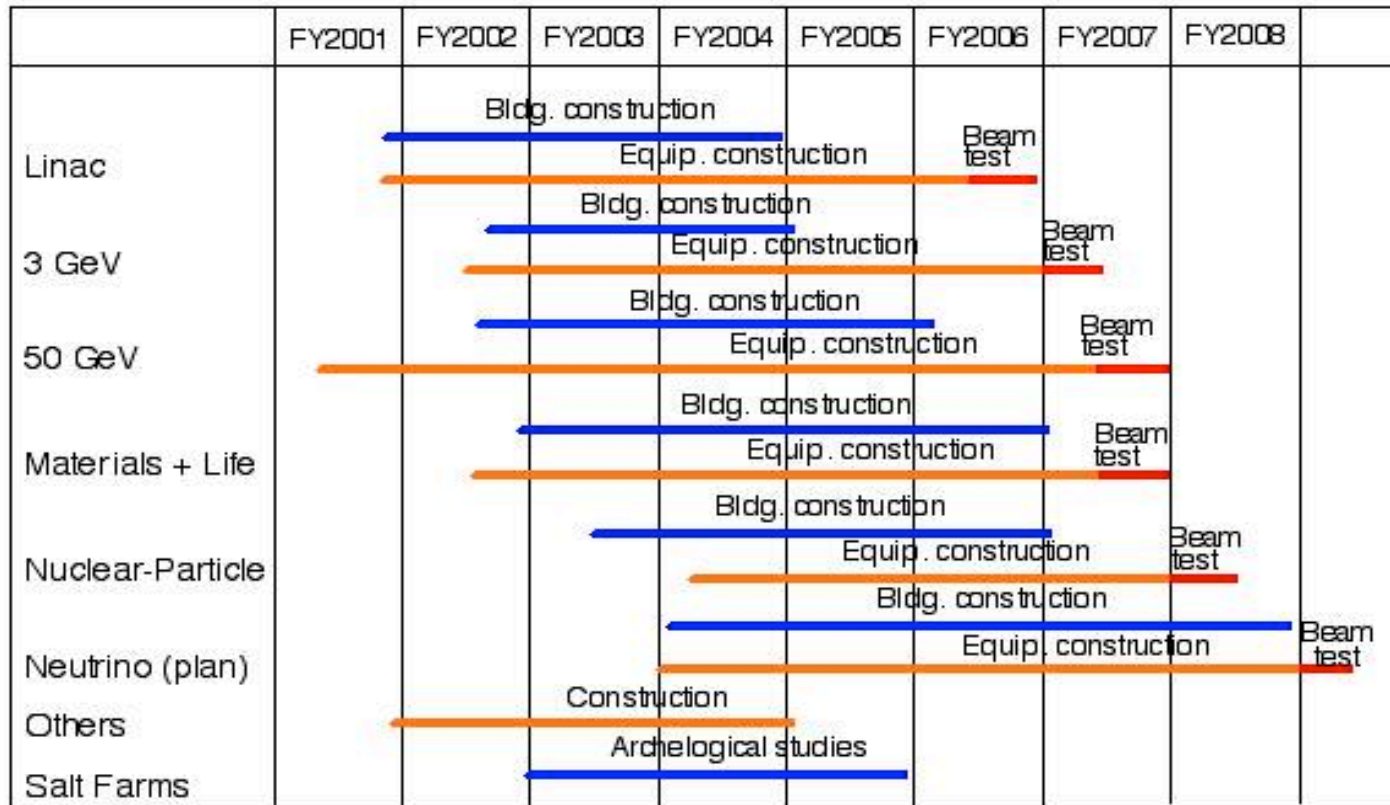
PDG (2002)	$L_{3,2j}$	Status	KA84 (1984)	( $^3P_0$ )model (1994)	SM95 (1995)	FA02 (2003)	Skyrme (1985)
Δ(1232)	$P_{33}$	****	1233(116)	1230	1233(114)	1233(118)	1424
Δ(1600)	$P_{33}$	***	1522(222)	1795	[1675-i193]	----	1435
Δ(1620)	$S_{31}$	****	1610(139)	1555	1617(108)	1614(141)	1478
Δ(1700)	$D_{33}$	****	1680(230)	1620	1680(272)	1688(365)	1737
Δ(1750)	$P_{31}$	*	----	1835	----	----	----
Δ(1750)	$F_{35}$	----	----	1910	----	----	----
Δ(1900)	$S_{31}$	***	1908(140)	2035	----	----	----
Δ(1905)	$F_{35}$	****	1905(260)	----	1850(294)	1856(334)	1931
Δ(1910)	$P_{31}$	****	1888(280)	1875	2152(760)	2333(1128)	1982
Δ(1920)	$P_{33}$	***	1868(220)	1915	----	----	1946
Δ(1930)	$D_{35}$	***	1901(195)	2155	2056(590)	2046(402)	1730
Δ(1940)	$D_{33}$	*	----	2080	----	----	----
Δ(1950)	$F_{37}$	****	1923(224)	1940	1921(232)	1923(278)	1816
----	$P_{33}$	----	----	1985	----	----	----
Δ(2000)	$F_{35}$	**	----	1990	----	----	----
----	$D_{33}$	----	----	2145	----	----	----
----	$D_{35}$	----	----	2165	----	----	----
Δ(2150)	$S_{31}$	*	----	2140	----	----	----
Δ(2200)	$G_{37}$	*	2215(400)	2230	----	----	2162
----	$G_{37}$	----	----	2295	----	----	----
----	$D_{35}$	----	----	2325	----	----	----
Δ(2300)	$H_{39}$	**	2217(300)	2420	----	----	2407
Δ(2350)	$D_{35}$	*	2305(300)	2265	----	----	----
Δ(2390)	$F_{37}$	*	2425(300)	2370	----	----	2083
Δ(2400)	$G_{39}$	**	2468(480)	2295	----	----	----
Δ(2420)	$H_{3,11}$	****	2416(340)	2450	----	----	2327
----	$F_{37}$	----	----	2460	----	----	----
----	$H_{39}$	----	----	2505	----	----	----

## 50GeV MR Main Parameters

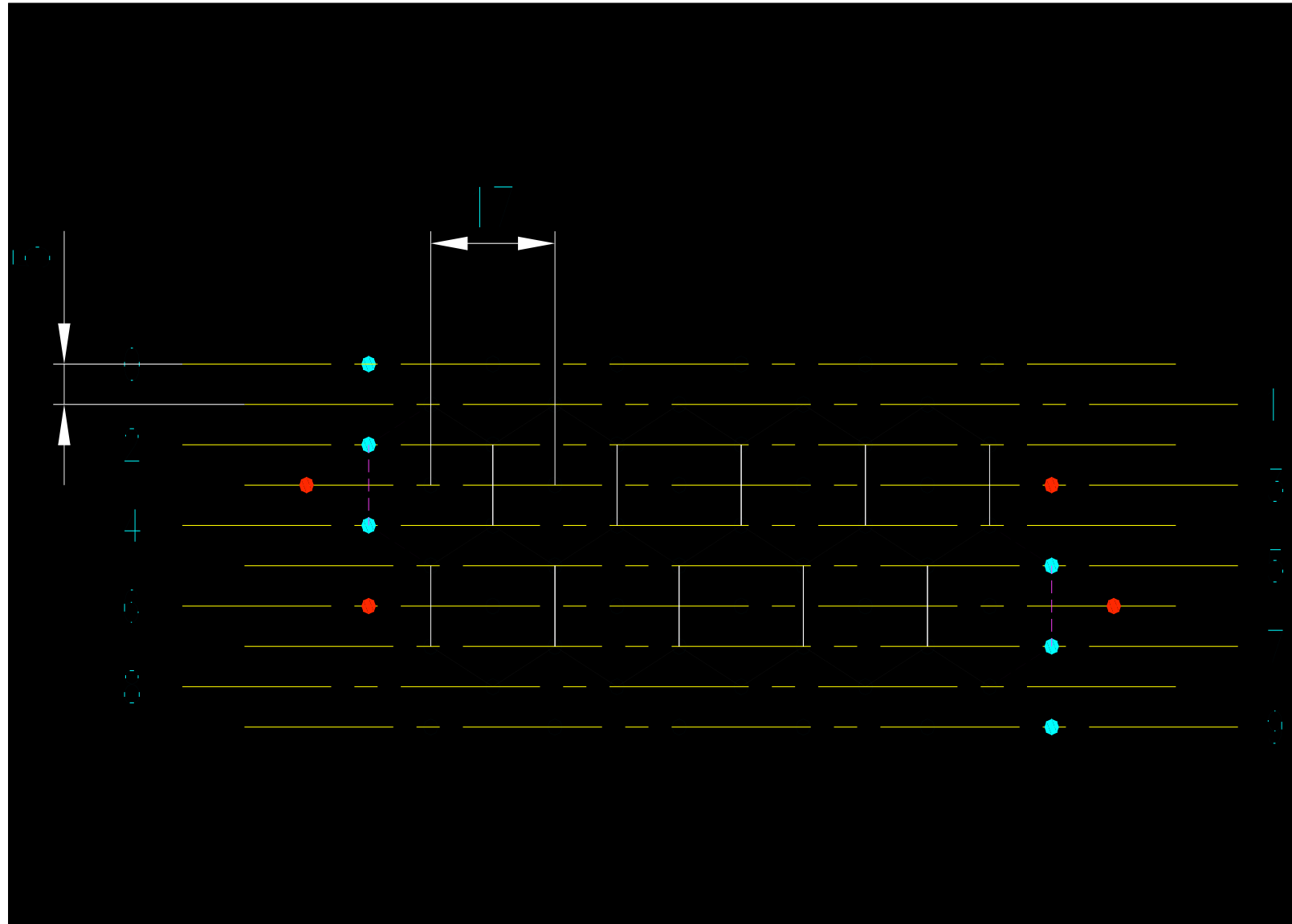
Parameters	Value
Circumference	1567.5 m
Average Radius	249.475 m
Injection Energy	3 GeV
Extraction Energy	50 GeV
Particle Per Pulse	$3.3 \times 10^{14}$
Revolution Period	
at Injection	5.384 $\mu$ s
at Extraction	5.230 $\mu$ s
Repetition Rate	0.3 Hz
Ramping Pattern	Parabola+Linear+Parabola
Injection	0.17 s
Acceleration	1.96 s
parabola	0.13 s
linear	1.7 s
parabola	0.13 s

# πN-πN in J-PARC

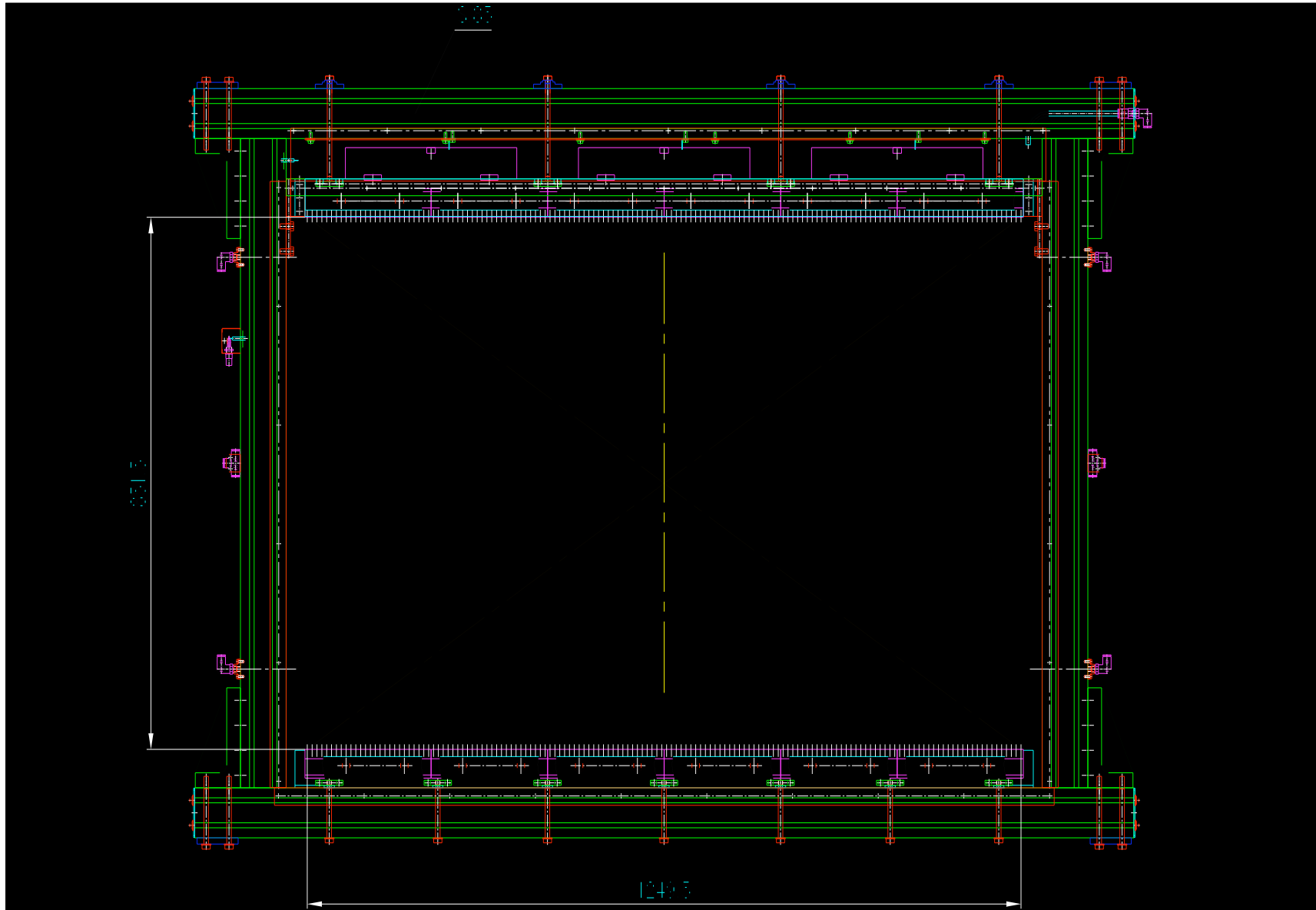
## Construction Schedule



# Drift chambers



# Drift chambers



## Polarized target

### Polarized proton target

#### 1. General description.

Polarized proton target with vertical spin orientation of polarized protons is used. More detailed description is given in the paper[1]. The target construction provides the possibility to rotate its cryostat around vertical axis. This allows to increase the window for outlet particles so that the setup possibilities can be improved substantially (fig. 1). Fig. 1 presents the view from above (in the plane of  $\pi$ N-elastic scattering). The section in the horizontal plane and possible scattering angles are shown.

---

[1] E.I. Bunyatova *et al.* Preprint PNPI-1191, 1986, 18 p.

Polarized target.

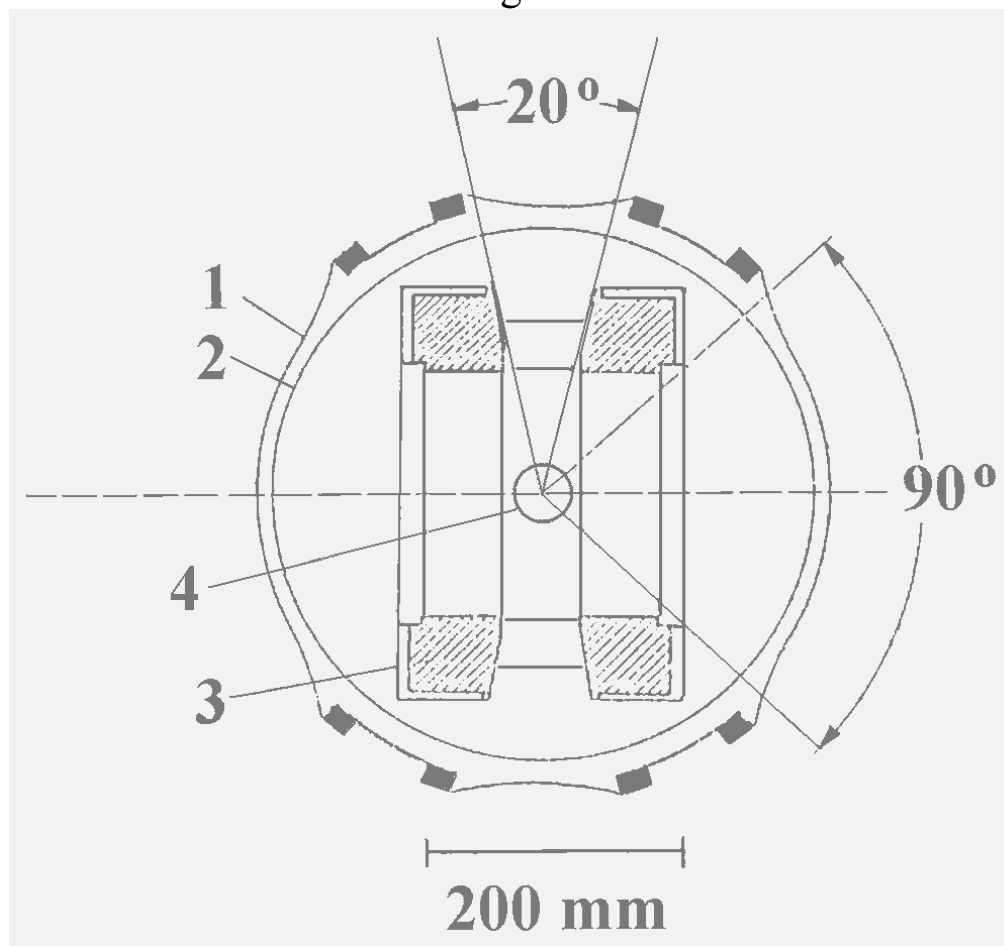
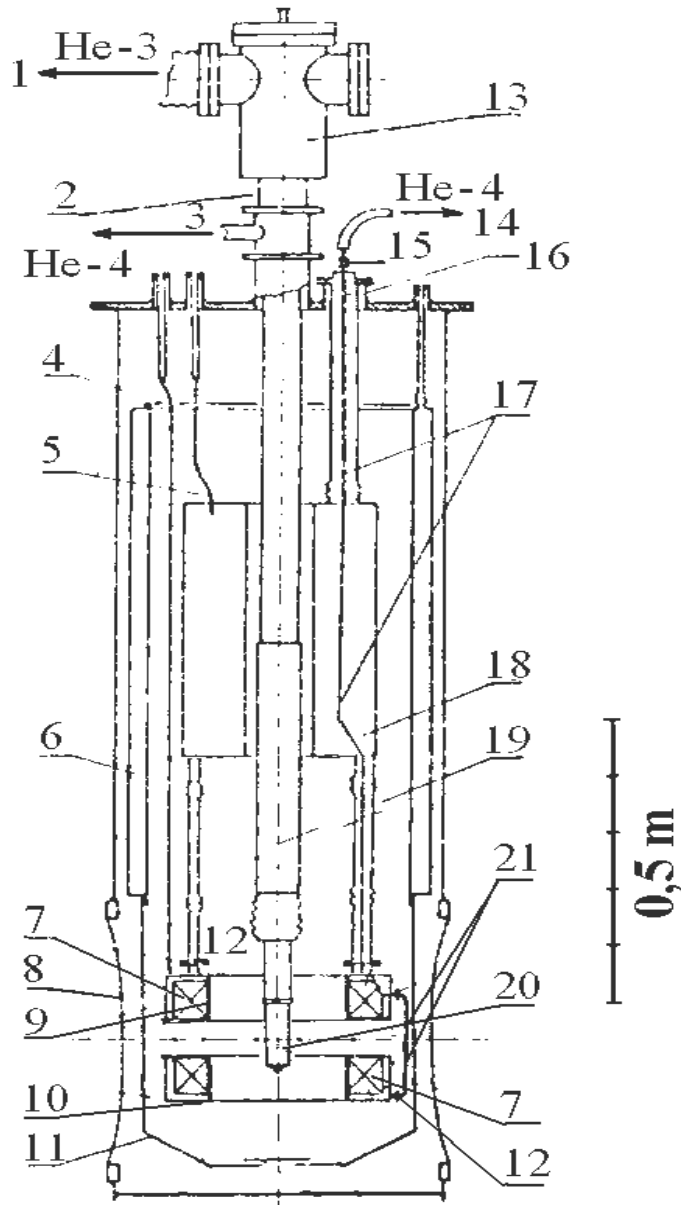


**Fig. 1.** Target: top view plane. There are shown:  
1 – target, 2 – nitrogen screen,  
3 – magnet area, 4 – container with the target properly.

## Polarized target

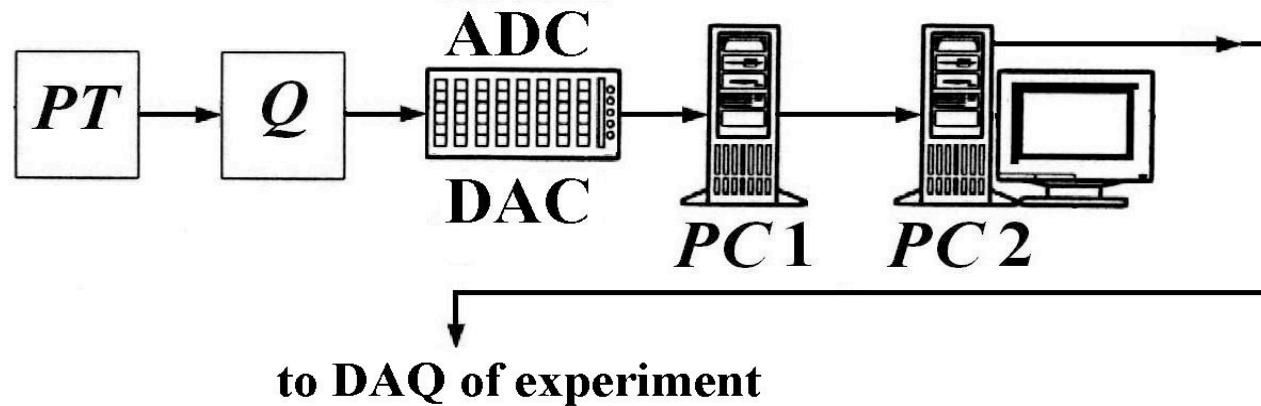


- Fig. 2.**  
Target in the vertical sectional view.
- 1 – helium-3 pump-out
  - 2 – neck
  - 3 – helium-4 pump-out
  - 4,11 – nitrogen screens
  - 5,21 – helium inputs
  - 6 – nitrogen tank
  - 7 – magnet
  - 8 – window
  - 9 – magnet frame
  - 10 – housing
  - 12 – indium compaction
  - 13 – rotating tee-joint
  - 14 – helium-4 output through current-input
  - 15 – connection to current source
  - 16 – current-input compaction and helium-4 output
  - 17 – current-input
  - 18 – helium tank (at 4.2 K)
  - 19 – refrigerator
  - 20 – appendix with target ( $C_3H_8O_2$ ) matter



## Electronic providing of the polarized target.

- ❖ the area under the PMR curve is determined using a  $Q$  meter
- ❖ the measuring circuit of which is excited by a high-frequency fixed-amplitude current
- ❖ Remote computer  $PC1$  contains a crate controller board and exercises direct control over the measuring system through the CAMAC crate
- ❖ An RF generator controlled by the sweep DAC produces a saw-tooth sweep
- ❖ ADC measures the voltage across the  $Q$  meter in each scanning cycle
- ❖ This system also comprises four adjustment DAC: tuning reference voltage phase, to adjust the measuring circuit, to select the PMR frequency (the RF generator frequency) and to control the magnetic field



u

## The experiment planning by the zero trajectory consideration.

ə

{ Barrelet method employment. }

The basic idea of the Barrelet methods is to represent the transverse amplitudes  $F_{\equiv}$  at fixed energy by the following ansatz, which exhibits the zeros in the complex  $z = \cos\theta_{cm}$  - plane:

u

$$F(\equiv; z) = F(1) \times \prod_{i=1}^N [(z - z_{\equiv_i}) / (1 - z_{\equiv_i}^*)] \times R(\equiv; z); \quad R(\equiv; 1) = 1.$$

as functions of a variable  $\omega$ , which is connected with  $z$  by a conformal mapping  $e^{i\theta} = z_{\equiv} = (z^2 - 1)^{1/2}$ . When  $\theta$  is real, it corresponds to the center-of-mass scattering angle. This mapping has the property, that a physical value of  $z$  (i.e.  $z$  real and  $|z| < 1$ ) is mapped onto two points in the  $\omega$ -plane, which lies on the upper and lower halves of the unit circle, respectively. Here  $\omega$  and  $\omega^{-1}$  belong to the same value of  $z$ .

ə

Transverse amplitudes have the advantage, that their modulus can be determined from  $d\sigma/d\Omega$  and  $P$  data alone  $|F_{\equiv}| = d\sigma/d\Omega \times (1 \mp P)$ .

d

This equation shows that the zeros of the amplitude can be derived from the zeros of  $d\sigma/d\Omega$  and  $P$  data but, unfortunately, there is a  $2^{2N}$  fold ambiguity because for each pair of zeros  $z_i$  and  $z_i^*$  (or  $\omega_i$  and  $1/\omega_i^*$ ) one has the choice whether  $z_i$  or  $z_i^*$  belongs to the amplitude  $F$ .

x

The spin rotation parameters  $A$  and  $R$  measurements can help in such choice.

ə

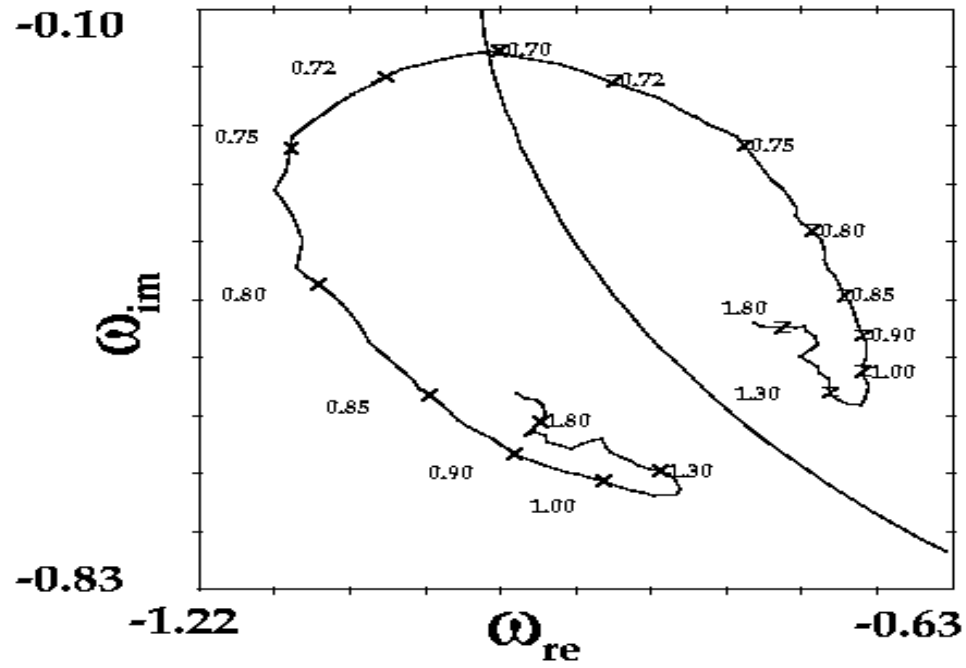
The positions of the zeros of  $F_{\equiv}$  depends of course on the incident pion beam momentum.

This allows one to locate problems of the unknown PWA ambiguities simply by looking at the zero trajectories on the  $\omega$ - planes which are near the physical region.

ə

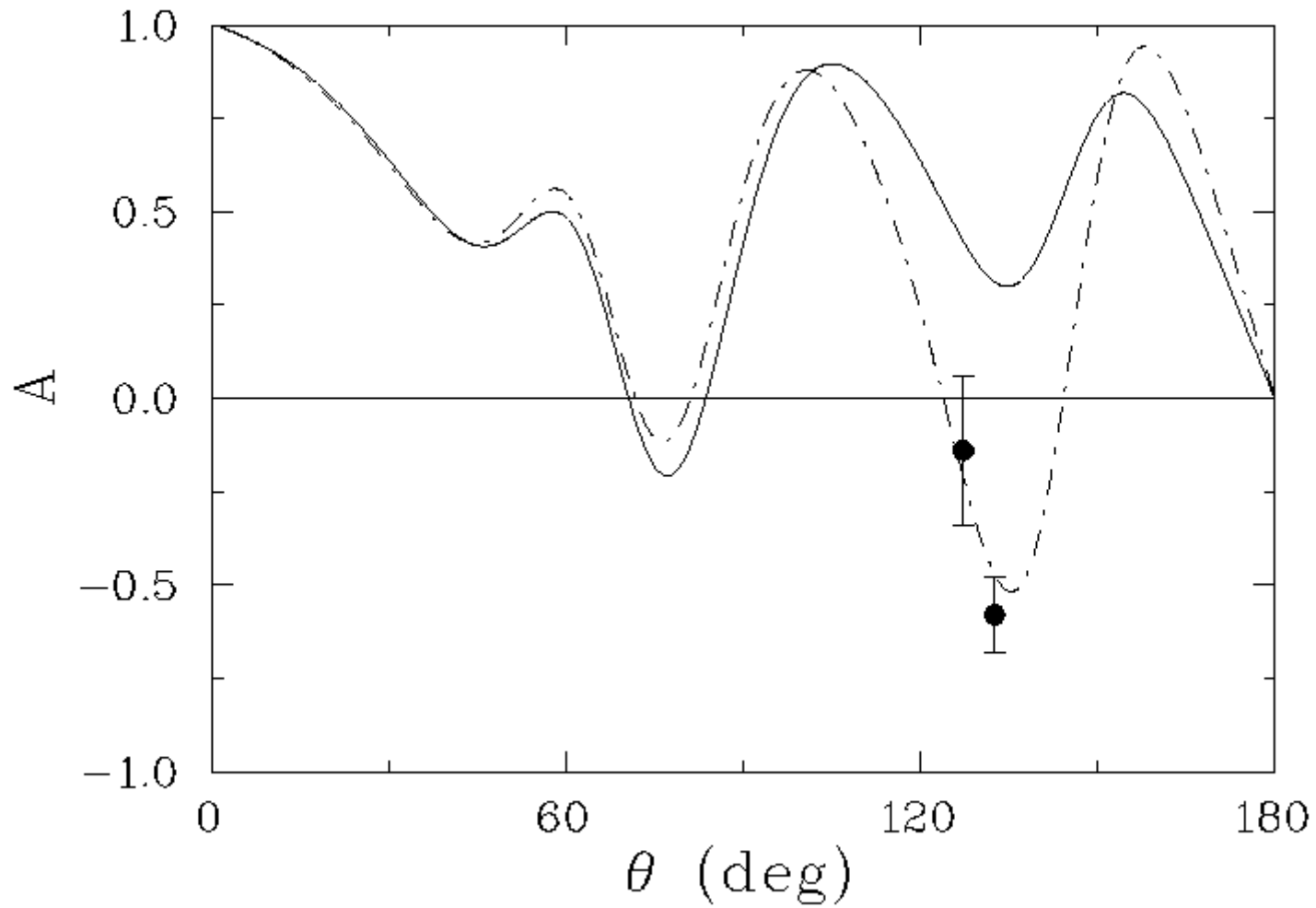
u

# Zero trajectories and experiment planning.

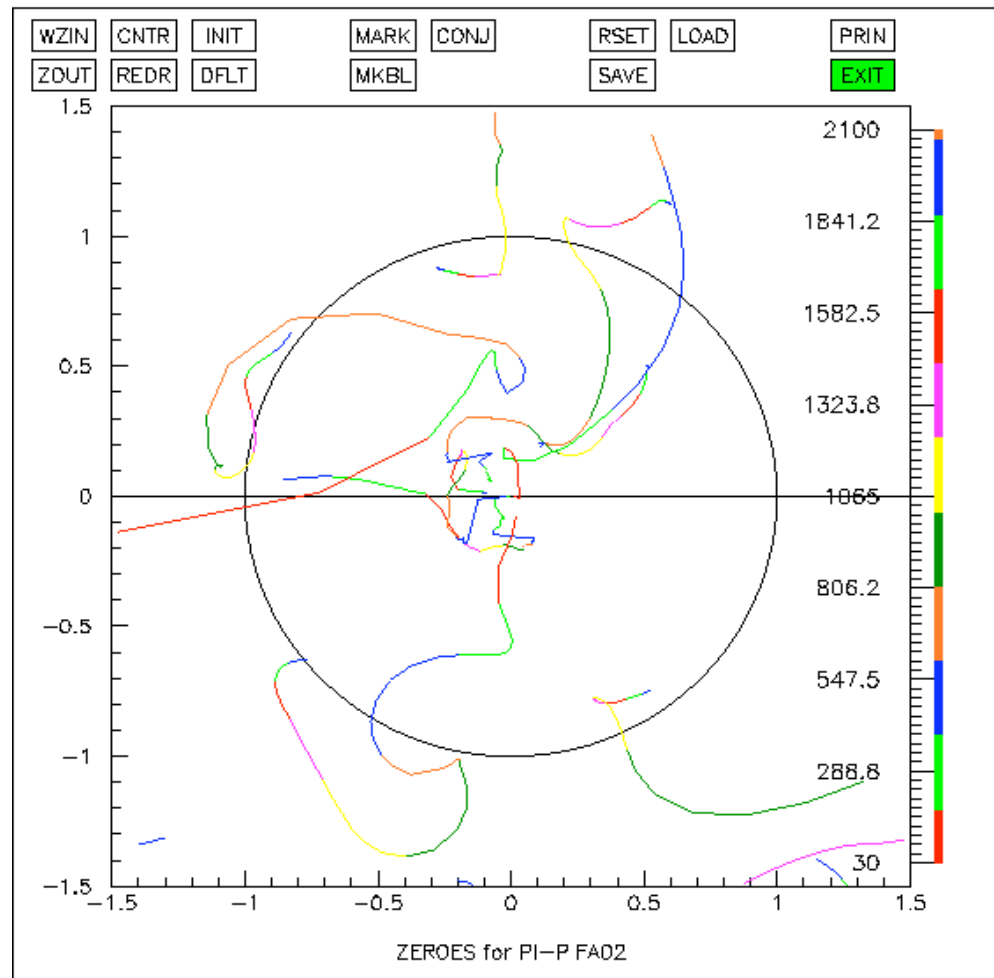


# Zero trajectories and experiment planning.

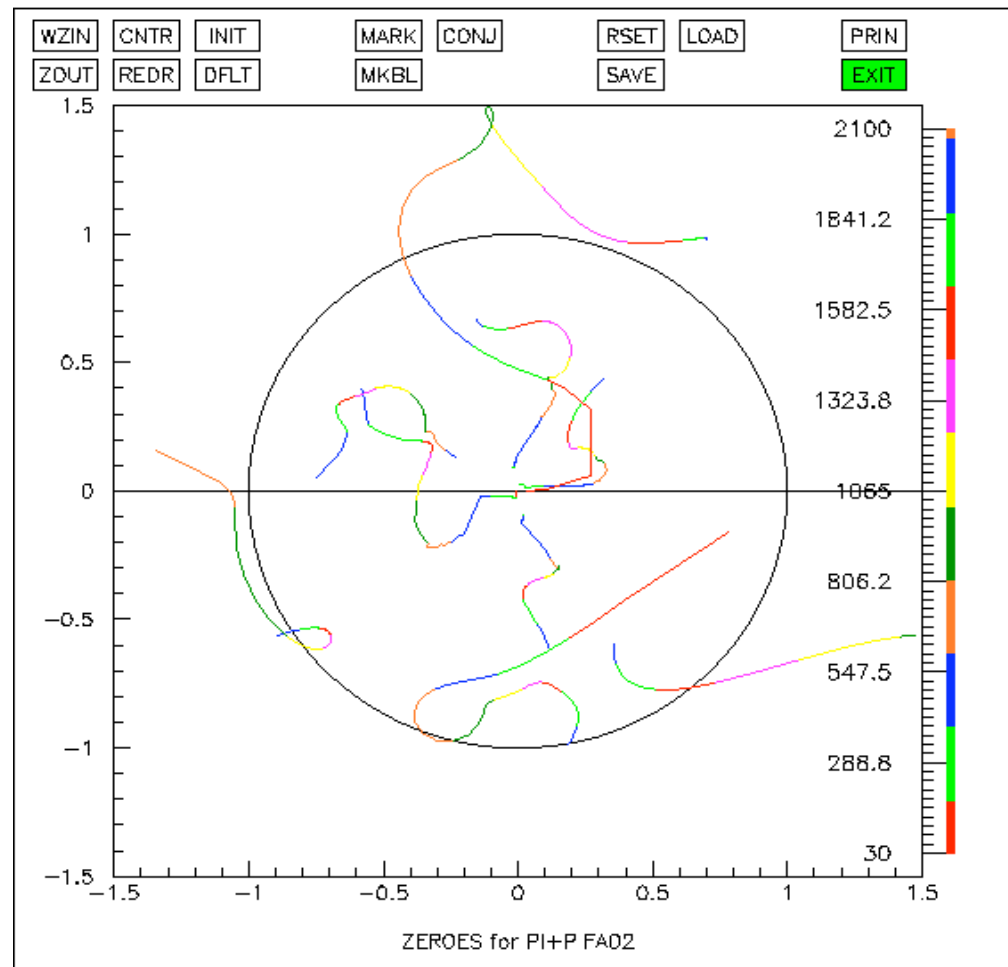
u  
e  
m  
!  
r  
e  
d  
x  
e  
e  
r



# Zero trajectories FA02.



# Zero trajectories FA02.



## Zero trajectories CMB.

